Unveiling the Intramolecular Ionic Diels-Alder Reactions within the Molecular Electron Density Theory

Luis R. Domingo,[1*] Mar Ríos-Gutiérrez,[1] and María José Aurell[1]

[1]Department of Organic Chemistry, University of Valencia, Dr. Moliner 50, E-46100 Burjassot, Valencia, Spain, E-mail: domingo@utopia.uv.es

Abstract

The intramolecular ionic Diel-Alder (IIDA) reactions of two dieniminiums have been studied within the Molecular Electron Density Theory (MEDT) at the ωB97XD/6-311G(d,p) computational level. ELF topological analysis of dieniminiums shows that its electronic structure can been seen as the sum of those of butadiene and ethaniminium. The superelectrophilic character of dieniminiums accounts for the high intramolecular global electron density transfer taking place between the diene and iminium frameworks at the transition state structures (TSs) of these IIDA reactions. The activation enthalpy associated to the IIDA reaction of the experimental dieniminium, 8.7 kcal·mol^{-1}, is closer to that of the ionic Diels-Alder (I-DA) reaction between butadiene and ethaniminium, 9.3 kcal·mol^{-1}. However, the activation Gibbs free energy of the IIDA reaction is 12.7 kcal·mol^{-1} lower than that of the intermolecular I-DA reaction. The strong exergonic character of the IIDA reaction, higher than 20.5 kcal·mol^{-1}, makes the reaction irreversible. These IIDA reactions present a total *re*/*exo* and *si*/*endo* diastereoselectivity, which is controlled by the most favourable chair conformation of the tetramethylene chain. Electron localization function (ELF) topological analysis of the single bond formation indicates that these IIDA reactions take place through a non-concerted *two-stage one-step* mechanism. Finally, ELF and atoms-in-molecules (AIM) topological analyses of the TS associated to inter and intramolecular processes show the great similitude among them.

Keywords: intramolecular ionic Diels-Alder reactions; Molecular Electron Density Theory; dieniminiums; superelectrophiles; global electron density transfer.

1. Introduction

The Diels-Alder (DA) reaction [1], which is one of a general class of cycloaddition reactions, is one of the most useful synthetic reactions in Organic Chemistry [2,3]. By varying the nature of the diene and the ethylene, many different types of six-membered carbocyclic structures can be built up. However, not all possibilities take place easily. For instance, the DA reaction between butadiene **1** and ethylene **2**, selected as the prototype of these cycloaddition reactions [4,5], must be forced to take place: after 17 h at 165 °C and 900 atm, a yield of 78% is obtained (see Scheme 1) [6].
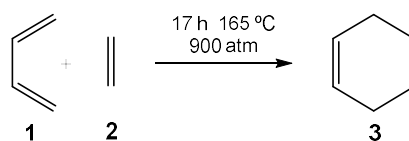
Scheme 1. DA reaction between butadiene **1** and ethylene **2**

Although this DA reaction is exothermic by 40 kcal/mol, it has a large activation energy of 27.5 kcal/mol [6]. For DA reactions, the negative activation entropy associated with these bimolecular processes also plays an adverse role. In this way, for the DA reaction between butadiene **1** and ethylene **2**, the activation entropy of the one-step process has been estimated to be -40.6 eu [7]. This unfavourable value, together with the high temperature required by the reaction, increases the activation Gibbs free energy of this DA reaction to 42.6 kcal/mol.

There are two different ways to reduce this unfavourable activation Gibbs free energy: (i) reduce the unfavourable activation enthalpy associated with the formation of the two new single bonds, and/or (ii) decrease the unfavourable activation entropy associated with these bimolecular processes.

An exhaustive theoretical study on experimental DA reactions, allowed establishing the definitive role of the global electron density transfer [8] (GEDT) taking place at the TSs in the feasibility of DA reactions [9,10]. This finding allowed establishing in 2009 the mechanism of the polar DA (P-DA) reactions [11], in which the favourable nucleophilic/electrophilic interactions taking place at the TSs is responsible for the feasibility of the reaction. The very good correlation found between the GEDT and the activation barriers for the DA reactions of Cp **4** with a series of 12 substituted ethylenes,

including iminium **5**, allowed the classification of the DA reactions in non-polar DA (N-DA), which do not take place easily experimentally, P-DA reactions, and ionic DA (I-DA) reaction, in which one of the two reagents is an ionic species (see Figure 1) [11]. Although, from the GEDT analysis it is not possible to stablish a clear separation between P-DA and I-DA reactions, these DA reactions have different behaviours.
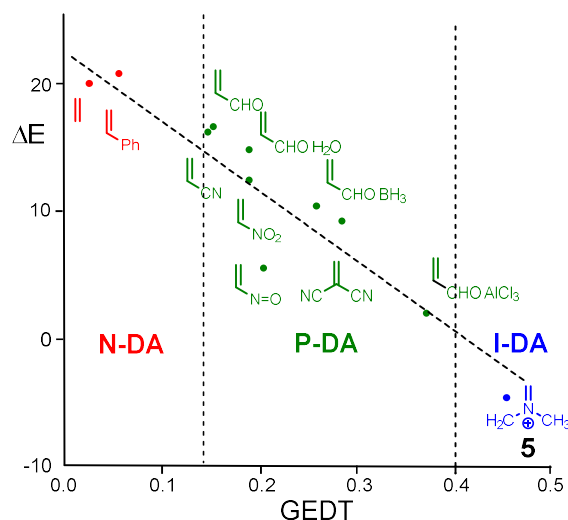

Figure 1. Plot of the activation barriers (ΔE in kcal·mol^{-1})) *vs.* the GEDT, e, $R^2 = 0.89$, for the DA reactions of Cp **4** with the substituted ethylene series of an increased electrophilic character. The classification of the DA reactions, based on the GEDT, is included

The I-DA reactions of a series of six iminiums **6** and **7** with Cp **4** have been recently studied within the Molecular Electron Density Theory [12] (MEDT) (see Scheme 2) [13]. The activation energies of these I-DA reactions were found between 13 and 20 kcal·mol^{-1} lower in energy than those associated to the corresponding P-DA reactions of neutral imines, as a consequence of the superelectrophilic character of iminiums, $\omega > 8.20$ eV. Unlike P-DA reactions, these I-DA reactions showed a low *endo* stereoselectivity as a consequence of the cationic character of the TSs, but highly regioselective [13]. In addition, polar solvents have poor effects on the relative energies, and an unappreciable effect in the geometries.
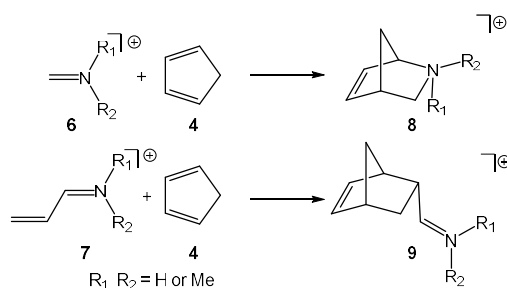
Scheme 2. I-DA reactions of iminiums **6** and **7** with Cp **4**

On the other hand, the unfavourable entropy cost associated to bimolecular processes may be overcome through an intramolecular process. Thus, in Table 1, the thermodynamic data for the N-DA reaction between butadiene **1** and ethylene **2** given in Scheme 1, and those for the intramolecular Diels-Alder (IMDA) reaction of (E)-deca-1,3,9-triene **10** given in Scheme 3 are given. The thermodynamic data of all species participating in these N-DA reactions are reported in Table S3 in the Supplementary Material.

The B3LYP/6-311G(d,p) activation enthalpy for the N-DA reaction between butadiene **1** and ethylene **2**, $\Delta H^{\#} = 25.7$ kcal·mol^{-1}, and the activation entropy, $\Delta S^{\#} = -44.8$ cal·mol^{-1}·K, are closer to the experimental values, 27.5 kcal·mol^{-1} and -40.6 cal·mol^{-1}·K, respectively [6,7]. These unfavourable values rise the activation Gibbs free energy of this intermolecular N-DA reaction computed at 165 ºC to 45.4 kcal·mol^{-1}. Despite the fact that the activation enthalpy associated to the IMDA reaction of **10**, $\Delta H^{\#} = 29.4$ kcal·mol^{-1}, is higher than that of the intermolecular one, the low activation entropy associated to this intramolecular process, $\Delta S^{\#} = -19.4$ cal·mol^{-1}·K, decreases the activation Gibbs free energy to 38.0 kcal·mol^{-1}. This behaviour explains the feasibility of non-polar IMDA reactions.
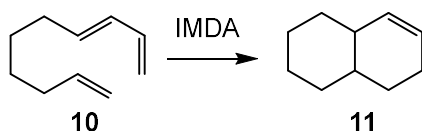

Scheme 3. IMDA reaction of (E)-deca-1,3,9-triene

Table 1. B3LYP/6-311G(d,p) Relative enthalpies (ΔH, in kcal·mol^{-1}), entropies (ΔS, in cal·mol^{-1}·K) and Gibbs free energies (ΔG, in kcal·mol^{-1}) computed at 165 ºC and 1 atm of the stationary points involved in the intermolecular N-DA reaction of butadiene **1** and ethylene **2**, and in the IMDA reaction of (E)-deca-1,3,9-triene **10**.

|	ΔH	ΔS	ΔG
TS-inter	25.7	-44.8	45.4
3	-28.5	-52.4	-5.5
TS-intra	29.4	-19.4	38.0
11	-28.8	-24.2	-18.2

Many theoretical studies devoted to non-polar and polar IMDA reactions can be found in the literature; however, only a small number of them have been devoted to intramolecular ionic Diels-Alder (IIDA) reactions.[14,15]

In 1988, Grieco and Parke used the IIDA reaction of dieniminium **12** in the synthesis of (−)-8a-epi-pumiliotoxin C **15** (see Scheme 4) [16]. The IIDA reaction of the generate *in situ* dieniminium **12** provided a mixture of the quinoliniums **13** and **14** in a ratio of 2.2 : 1. Quinolinium **13** was further converted into **15** upon a hydrogenation reaction.
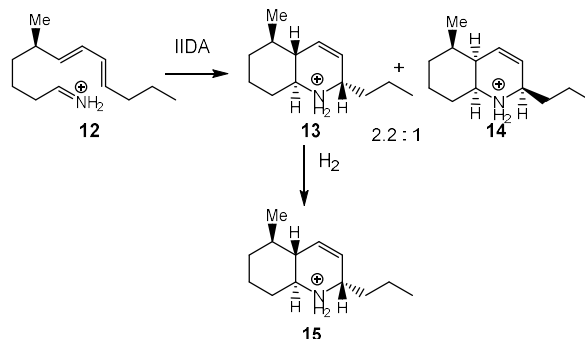
Scheme 4. IIDA reaction of dieniminium **12** experimentally studied by Grieco and Parke [16]

Herein, an MEDT study of the IIDA reaction of dieniminium **12**, experimentally studied by Grieco and Parke [16], is performed in order to understanding the behaviours of the IIDA reactions (see Scheme 4). To this end, the I-DA reaction of butadiene **1** with iminium **18**, and the IIDA reaction of (E)-nona-6,8-dien-1-iminium **16**, as a reduced model of dieniminium **12**, have been also studied (see Scheme 5).
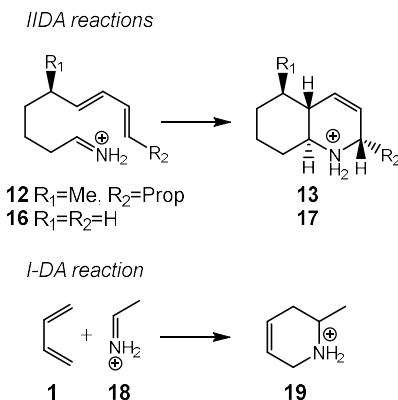
Scheme 5. IIDA reactions of dieniminiums **12** and **16**, and I-DA reaction of butadiene **1** with iminium **18** herein studied

2. Computational Methods

DFT calculations were performed using the hybrid ωB97X-D functional [17], which includes long range exchange (denoted by X) correction as well as the semiclassical London-dispersion correction (indicated by suffix-D). The standard 6-311G(d,p) basis set was used [18], which includes d-type polarization for second row elements and p-type polarization functions for hydrogen atoms. The Berny method was used in optimizations [19,20]. Only one imaginary frequency characterized all studied TSs. The intrinsic reaction coordinate (IRC) paths [21] were carried out to find the unique connection given between the TSs and the minimum stationary points [22,23]. Solvent effects of ethanol were considered by full optimization of the gas phase structures at the same computational level using the polarizable continuum model [24,25] (PCM) in the framework of the self-consistent reaction field [26-28] (SCRF).

The GEDT [8] values were estimated by a NPA [29,30], using the equation GEDT (f) = $\sum_{q \in f} q$, were q are the atoms of a framework (f) at the TSs. CDFT reactivity indices [31,32] were calculated through the equations given in reference [32]. All calculations were carried out with the Gaussian 16 suite of programs [33].

The topology of the electron localization function [34] (ELF) of the ωB97XD/6-311G(d,p) monodeterminantal wavefunctions was carried out using the TopMod [35] package with a cubical grid of step size of 0.1 Bohr. The Bader's quantum theory of atoms-in-molecules [36] (AIM) analyses were conducted using Multiwfn 3.7 software packages [37]. GaussView program [38] was used to visualize molecular geometries of all the systems as well as the position of the ELF basin attractors. The ELF localization domains at an isovalue of 0.75 a.u. were obtained with the Paraview software [39,40].

3. Results and Discussions

The present MEDT study has been divided into three parts: i) first, a study of the electronic structure and reactivity at the ground state (GS) of the reagents is performed; ii) in the second part, the study of the reaction paths associated to I-DA reaction between butadiene **1** and ethaniminium **18**, and those associated to the IIDA reactions of dieniminiums **12** and **16** is carried out; and finally, iii) in the third part, a topological analysis of the bonding changes along the IIDA reactions of dieniminiums **12** is

presented. A comparative ELF and AIM topological analysis of the most favorable TSs involved in the inter and intra I-DA reactions is also performed.

3.1. Study of the structure and reactivity at the GS of the reagents.

3.1.1. Analysis of the GS electronic structures of the reagents

The topological analysis of the ELF [34] allows a quantitative and qualitative characterization of chemical regions of a molecule [41]. Thus, the topology of the ELF of butadiene **1**, ethaniminium **18** and dieniminium **16** was first studied in order to characterize their electronic structures. Due to the free C−C single bond rotation of the tetramethylene chain of dieniminium **16**, this species can be found as a series of conformers, also named rotamers. Only two conformations have been selected in the present study: i) the extended conformation, denoted as **16e**, in which all methylenes CH_2 of the tetramethylene chain are positioned in alternate conformations, and ii) the fold conformation, denoted as **16f**, which open the reaction path for the IIDA reaction. The ELF basin attractor positions of **1**, **18** and **16e** are shown in Figure 2. The ELF basin attractor positions of dieniminium **12e** are shown in Figure S3 in Supplementary Material.

The ELF analysis of butadiene **1** shows the presence of two pairs of disynaptic basins, V(C3[5], C4[6]) and V'(C3[5], C4[6]), integrating a total population of 3.38 e each one, associated to a two depopulated C3[5]−C4[6] double bonds, and one V(C4,C5) disynaptic basin, integrating 2.20 e, associated to a populated C4−C5 single bond. On the other hand, the ELF analysis of ethaniminium **18** shows the presence of two disynaptic basins, V(N1,C2) and V'(N1,C2), integrating a total of 3.42 e, associated to a depopulated N1−C2 double bond.
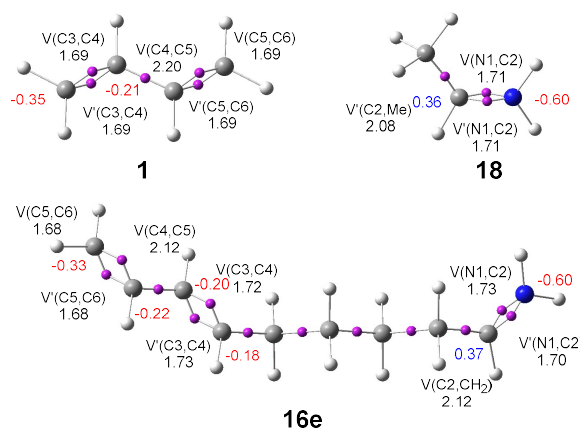

Figure 2. ELF basin attractor positions together with the most relevant valence basin populations, and natural atomic charges, in average number of electrons e, blue colour is

used for positive charges and red colour for negative ones, of butadiene **1**, ethaniminium **18** and dieniminium **16e**

The ELF analysis of dieniminium **16e** shows the presence of two disynaptic basin, V(N1,C2) and V'(N1,C2), integrating a total of 3.43 e associated to the N1−C2 double bond of the iminium framework, and two pairs of disynaptic basins, V(C3[5], C4[6]) and V'(C3[5], C4[6]), integrating a total population of ca 3.4 e each one, and one V(C4,C5) disynaptic basin, integrating 2.12 e, associated to the butadiene C3−C4−C5−C6 framework. The tetramethylene chain joining the butadiene and iminium frameworks is characterized by the presence of three V(Ci,Cj) disynaptic basins, integrating between 1.70e and 1.86 e. ELF of dieniminium **16e** indicates that the electronic structure of this species can be seen as the addition of the electronic structure of butadiene **1**, plus that of ethaniminium **18**, and plus that of the tetramethylene chain. ELF of experimental dieniminium **12e** is identical to that of **16e** (see Figure S3 in Supplementary material).

The natural atomic charges [29,30] are given in Figure 2. At ethaniminium **18**, while the C2 carbon is positively charged by 0.36 e, the N1 nitrogen is negatively charged by −0.60 e [13]. At dieniminium **16e**, the N1 nitrogen and C3 carbon present a same charge distribution than that at ethaniminium **18**. Only, the C3 carbon of dieniminium **16e** presents a lower negative charge, −0.18, as a consequence of the substitution of a hydrogen at ethaniminium **18** by a methylene at **16e**. Interestingly, while the Lewis structures of iminiums localize the positive charge at the nitrogen atom, it is negatively charged [13].

3.1.2. Analysis of the CDFT reactivity indices at the GS of the reagents.
Many studied devoted to cycloaddition reactions have proof that the analysis of the global and local reactivity indices defined within the CDFT [31,32] is a powerful tool to understand polar reactions [42,43]. The CDFT indices were obtained at the B3LYP/6-31G(d) computational level due to it was used to define the scales of electrophilicity and nucleophilicity [32]. The global reactivity indices of the reagents participating in the I-DA and IIDA reactions herein studied are collected in Table 2.

Table 2. B3LYP/6-31G(d) Global reactivity indices, the electronic chemical potential, μ, chemical hardness, η, electrophilicity, ω, and nucleophilicity, N, in eV, of the reagents participating in the I-DA and IIDA reactions herein studied.

	μ	η	ω	N
12e	-7.39	1.02	26.72	1.22
16e	-7.65	1.16	25.19	0.89
16f	-8.23	3.76	9.01	-0.99
ethaniminium **18**	-11.82	8.27	8.46	-6.83
12f	-7.85	3.68	8.36	-0.57
butadiene **1**	-3.42	5.62	1.04	2.89
pentadiene **20**	-3.17	5.51	0.91	3.20
dienimine **21**	-3.31	5.47	1.00	3.08

The electronic chemical potential [31,44] μ of butadiene **1**, μ = −3.42 eV, is higher than that of ethaniminium **18**, μ = −11.82 eV. Consequently, it is expected that along the corresponding I-DA reaction, a mount the electron density will be transferred from butadiene **1** to ethaniminium **18**, the reaction being classified of the forward electron density flux (FEDF) [45].

The electrophilicity ω index [46] of the iminiums ranges from 8.36 (**12f**) to 26.72 (**12e**) eV, being classified as strong electrophiles within the electrophilicity scale [32]. The electrophilicity ω index of iminium **12f**, 8.36 eV, is closer to that of ethaniminium **18**, 8.46 eV, being both classified as superelectrophiles [47]. As expected, the nucleophilicity N index [48] of these species range from −6.83 (**18**) to 1.12 (**12e**) eV, being classified as marginal nucleophiles within the nucleophilicity scale [32].

Interestingly, the extended conformations of dieniminiums **12e** and **16e** present anomalous electrophilicity ω values, 26.72 (**12e**) and 25.19 (**16e**) eV, respectively, when they are compared with the values of the fold conformations **12f** and **16f**. Analysis of the reactivity indices of these species indicates that they present a very low hardness, lesser of 1.20 eV (see Table 2). As the hardness η is found in the denominator of the equation defining the electrophilicity ω index (see equation 1) [46], a decrease of the hardness η provokes a noticeable increase of the electrophilicity ω index. On the other hand, the hardness η is approached to the HOMO-LUMO gap (see equation 2) [31]. The presence of the iminium and the diene frameworks in these species decreases and increases notably the LUMO and HOMO energies, respectively, thus causing an unexpected very low value for the hardness η, and, consequently, a very high value for the electrophilicity ω index.

$$\omega = \frac{\mu^2}{2\eta} \tag{1}$$

$$\eta \approx (E_{LUMO} - E_{HOMO}) \tag{2}$$

A good correlation between the electrophilicity ω indices and the LUMO energies, ε_{LUMO}, for the ten substituted ethylenes given in Figure 1 is established in Section 1 in Supplementary Material. This correlation allows establishing the polynomic equation 3, which permits to estimate the electrophilicity ω through LUMO energies, ε_{LUMO}:

$$\omega_{LUMO} = 0.059 * \varepsilon_{LUMO}^2 - 0.5803* \varepsilon_{LUMO} + 0.8589 \tag{3}$$

By using the proposed equation 3, the electrophilicity ω_{LUMO} index for the extended conformations of dieniminiums **12** and **16** are estimated in 7.64 eV for **12e**, and 7.91 eV for **16e** (see Table S2), which are in reasonable agreement with the values computed for the fold conformations of dieniminiums **12** and **16**: 8.36 eV or **12f** and 9.91 eV for **16f**.

Butadiene **1** has an electrophilicity ω and nucleophilicity N indices of 1.04 and 2.89 eV, respectively, being classified as a moderate electrophile and in the borderline of moderate nucleophile. Inclusion of an electron-releasing methyl group on butadiene increases the nucleophilicity N index of pentadiene **20** to 3.20 eV, being classified as a strong nucleophile. This value is closer to that of dienimine **21**, $N = 3.08$ eV, the deprotonated iminium **16**. Consequently, the I-DA reaction between ethaniminium **18** and pentadiene **20** will be characterized also by a high GEDT.

DA reactions involving asymmetric electrophilic compounds take place via asynchronous TSs [10,13]. The most favourable two-center interactions between the two interacting species in polar and ionic processes takes place between the most electrophilic center of the electrophile, and the most nucleophilic center of the nucleophile [49]. In this context, the electrophilic P_k^+ and nucleophilic P_k^- Parr functions [50] derived from the excess of spin electron density reached via the GEDT [8] process from the nucleophile toward the electrophile have shown to be one of the most accurate and insightful tools for the study of the local reactivity in polar and ionic processes. On the other hand, analysis of the electrophilic P_k^+ and nucleophilic P_k^- Parr functions in intramolecular cycloaddition

reactions allows characterising the electrophilic and nucleophilic centres of the reactant molecules [51]. Consequently, the electrophilic P_k^+ and nucleophilic P_k^- Parr functions of the model dieniminium **16e** were calculated and analysed. The corresponding values are given in Figure 3.

Analysis of the electrophilic P_k^+ Parr functions of dieniminium **16e** shows that they are manly concentrated on the N=C iminium framework. Thus, the iminium C2 carbon, with a $P_k^+ = 0.83$, concentrates more than the 80 % of the electrophilicity of this species. On the other hand, the nucleophilic P_k^- Parr functions of dieniminium **16e** shows that they are manly concentrated on the C3, $P_k^- = 0.40$, and C6, $P_k^- = 0.47$, carbons of the butadiene framework. Although the most favourable two-centre interactions along the IIDA reactions will be that between the C2 and C6 centres, it will provoke a strong geometrical distortion. Consequently, along the intramolecular process, the best two-centre interaction will take place between the C2 and C3 centres.
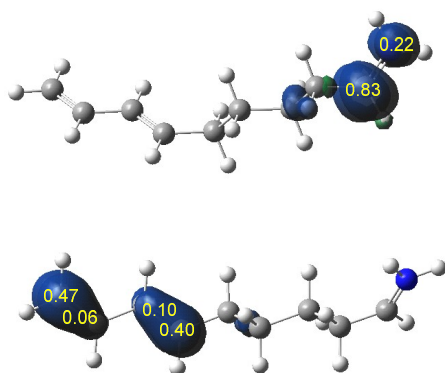

Figure 3. 3D representations of the Mulliken atomic spin densities of the neutral radical and radical cation of the reduced model dieniminium **16e**, and the electrophilic P_k^+ and nucleophilic P_k^- Parr functions.

3.2.1. Study of the intermolecular I-DA reaction between butadiene 1 and ethaniminium 18.

In order to understand the IIDA reaction of dieniminium **12** (see Scheme 6), the I-DA reaction between butadiene **1** and ethaniminium **18** was first studied. This I-DA can take place *via* two stereoisomeric reaction paths, the *endo* and the *exo*. Along the *endo* approach mode, the methyl group of ethaniminium **18** is positioned above the diene system of butadiene **1**. Analysis of the stationary points found along the two reaction paths indicates that this I-DA relation takes place through a one-step mechanism. Consequently, two TSs, **TS1-n** and **TS1-x**, and the corresponding cycloadducts **22** and

23 were located and characterised. The relative energies in ethanol are given in Table 3, while the total energies are given in Table S4 in Supplementary Material.
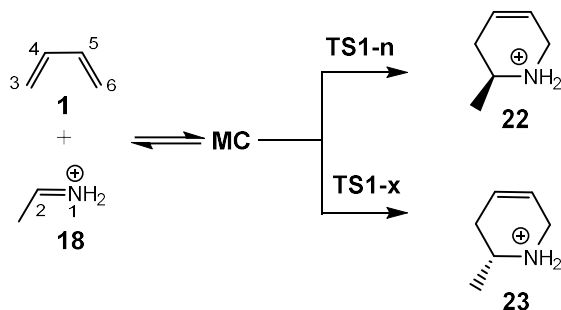
Scheme 6. I-DA reaction between butadiene **7** and ethaniminium **8**

At the begin of the reaction, a series of molecular complexes (MCs) can be found. They are characterised by the presence of weak electronic interactions between butadiene **1** and iminium **18**. Only the most stable **MC** was selected as energy reference. **MC** is found 4.5 kcal·mol^{-1} below the separated reagents. The relative enthalpies of the TSs with respect the reagents are 8.1 (**TS1-n**) and 9.0 (**TS1-x**) kcal·mol^{-1}; the reaction being exothermic by more than 35.9 (**23**) kcal·mol^{-1}.

Some appealing conclusions can be drawn from the energy results given in Table 3: i) formation of **MC** is an exothermic process. However, if the thermal correction and the entropies are considered, they become endergonic 6.0 kcal·mol^{-1}; ii) in ethanol, this I-DA reaction present an activation energy of 8.1 kcal·mol^{-1}. Note that in gas phase the TSs are found below the separated reagents [13]; iii) this I-DA reaction presents a low *endo* stereoselectivity as **TS1-x** is found only 0.9 kcal·mol^{-1} above **TS1-n**; and iv) this I-DA reaction is highly exothermic, higher than 36 kcal·mol^{-1}.

Table 3. ωB97XD/6-311G(d,p) relative electronic energies (ΔE, in kcal·mol^{-1}), enthalpies (ΔH, in kcal·mol^{-1}), entropies (ΔS, in cal/mol.K) and Gibbs free energies (ΔG, in kcal·mol^{-1}) computed at 75 ºC and 1 atm in ethanol, of the stationary points involved in the I-DA reactions of butadiene **1** with ethaniminium **18**.

	ΔE	ΔH	ΔS	ΔG
MC	-4.5	-3.1	-26.0	6.0
TS1-n	8.1	9.3	-46.1	25.3
TS1-x	9.0	10.1	-44.9	25.8
22	-41.3	-36.3	-51.6	-18.3
23	-35.9	-31.0	-49.9	-13.6

The thermodynamic data of the I-DA reaction between butadiene **1** and ethaniminium **18** were them analysed. Relative enthalpies, entropies and Gibbs free energies, computed at 75 ºC in ethanol, are given in Table 3. Inclusion of the thermal corrections to the electronic energies in ethanol decreases the relative enthalpies between 1.1 and 5.1 kcal·mol^{-1}. The lower incidence takes place in the relative enthalpies of TSs which decrease by only 1.1 kcal·mol^{-1} with respect to the electronic energies in ethanol. The inclusion of the thermal corrections and entropies to enthalpies increases the relative Gibbs free energies between 8 and 18 kcal·mol^{-1} as a consequence of the unfavourable activation entropy associated to this bimolecular process, between −26 and −46 cal·mol^{-1}·K^{-1}. Thus, the activation Gibbs free energy associated to this I-DA reaction in ethanol rises to 25.3 kcal·mol^{-1}, while formation of **22** becomes exergonic by −18.3 kcal·mol^{-1}. The activation Gibbs free energy associated to this I-DA reaction is 20.1 kcal·mol^{-1} lower than that associated to the N-DA reaction between butadiene **1** and ethylene **2** (see Table 1) as a consequence of the high GEDT taking place at the I-DA reaction (see later) [13]. It is important to remark that while formation of **MC** is exothermic by 3.1 kcal·mol^{-1}, it is endergonic by 6.0 kcal·mol^{-1} as a consequence of the unfavourable negative entropy associated to its formation, −26.0 cal·mol^{-1}·K^{-1} (see Table 3).

The geometries of **TSint-n** and **TSint-x** involved in the I-DA reaction of butadiene **1** with ethaniminium **18** are given in Figure 4. The distances between the C2−C3 and N1−C6 interacting centers at the TSs are: 1.894 and 2.761 Å at **TS1-n**, and 1.905 and 2.793 Å at **TS1-x**. These geometrical parameters indicate that these TSs are associated to high asynchronous single bond formation processes. Considering that the C−C single bond formation takes place in the range 2.0 − 1.9 Å [8], the C2−C3 distances indicate that at these TSs the formation of the corresponding C2−C3 single bond has begun yet.
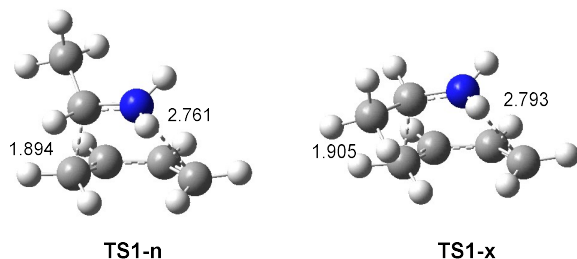

Figure 4. ωB97XD/6-311G(d,p) geometries of **TS1-n** and **TS1-x**. The C−C and C−N distance are given in Angstroms.

The ionic nature of this I-DA reaction was evaluated by computing the GEDT values at the TSs. The computed GEDT values at the corresponding TSs, which fluxes from the nucleophilic butadiene **1** to the superelectrophilic iminium **18** are 0.46 e at **TS1-n** and **TS1-x**. These very high values point out the high GEDT taking place at this I-DA reactions, which classify it as of FEDF [45].

3.2.2. Study of the IIDA reactions of dieniminiums 12 and 16

The IIDA reactions of dieniminiums **12** and **16** can take place through four competitive reaction paths (see Scheme 7). They are related to the *endo* and *exo* approach modes of the iminium framework with respect to the diene system, named as *n* and *x*, and through the *pro-re* and *pro-si* faces of the C3 carbon of the butadiene system, named as *r* and *s*. Analysis of the stationary points found along the four reaction paths indicates that these IIDA reactions take place through a one-step mechanism. Consequently, four TSs, **TS2(3)-rn**, **TS2(3)-rx**, **TS2(3)-sn** and **TS2(3)-sx**, and the corresponding quinoliniums were located and characterised for each IIDA reaction. The relative energies in ethanol are given in Table 4, while the total energies are given in Table S5 Supplementary Material.
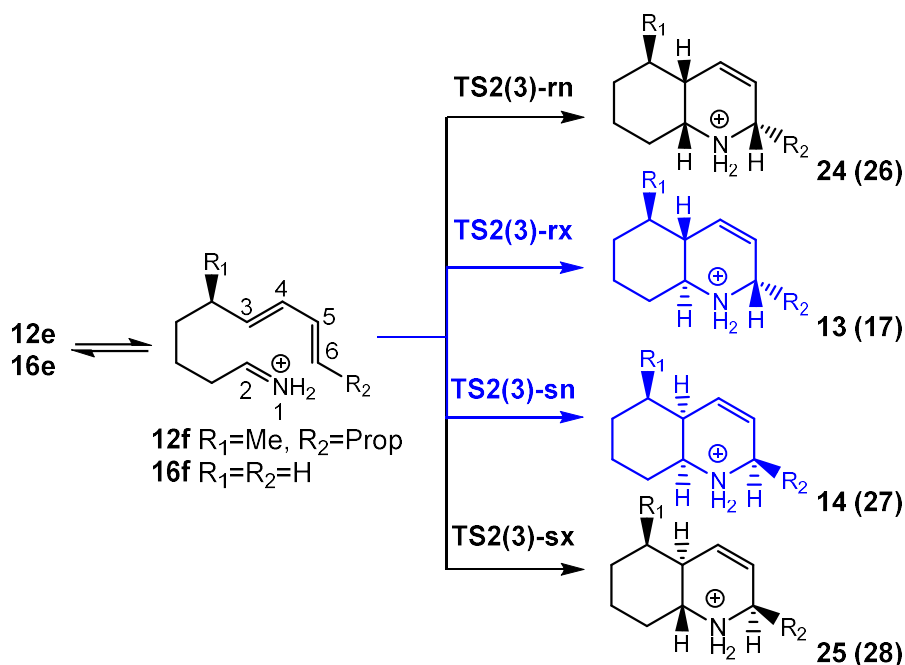
Scheme 7. Competitive reaction paths associated with the IIDA reactions of dieniminiums **12** and **6**

Dieniminiums **12** and **16** can exist in several conformations resulting from the free rotation of the C−C single bonds of the tetramethylene chain. For these dieniminiums, two conformations were considered; the fold **12f** and **16f**, and the extended **12e** and **16e** conformations. The activation energies in ethanol associated to these IIDA reactions ranges from 8.8 (**TS2-rx**) to 13.9 (**TS2-sx**), and from 13.6 (**TS3-rx**) to 18.1 (**TS3-sx**) kcal·mol^{-1}, the reactions being strongly exothermic by more than 27 kcal·mol^{-1}.

Some appealing conclusions can be obtained from the relative energies given in Table 4: i) while for the experimental dieniminium **12** the fold conformation **12f** is found 0.3 kcal·mol^{-1} below the extended conformation **12e**, for the dieniminium model **16** the extended conformation **16e** is found 1.0 kcal·mol^{-1} below the fold conformation **16f**; ii) the activation energy associated to the IIDA reaction of experimental dieniminium **12**, 8.8 (**TS2-rx**) kcal·mol^{-1}, is 4.8 kcal·mol^{-1} lower in energy than that associated to the IIDA reaction of dieniminium **16**, 13.6 (**TS3-sn**) kcal·mol^{-1}; the IIDA reaction of dieniminium **12** presents a closer activation energy than that of the intermolecular process (see Table 3); iii) these IIDA reactions present a high *exo* selectivity along the *re* approach mode, and a high *endo* selectivity along the *si* approach mode; iv) formation of quinolinium **13** via **TS2-rx** is only 0.1 kcal·mol^{-1} more favourable than formation of quinolinium **14** via **TS2-sn**, while formation of quinoliniums **24** and **25** is kinetically unfavoured in agreement with the experimental outcomes [14]; and finally v) formation of quinoliniums **13** and **14** are exothermic by more than 30 kcal·mol^{-1}.

Table 4. ωB97XD/6-311G(d,p) relative energies (ΔE, in kcal·mol^{-1}, with respect to the most stable conformation) in ethanol of the stationary points involved in the IIDA reactions of dieniminiums **12** and **16**.

	ΔE		ΔE
12e	0.3	**16e**	0.0
12f	0.0	**16f**	1.0
TS2-rn	12.9	**TS3-rn**	17.7
TS2-rx	8.8	**TS3-rx**	13.6
TS2-sn	8.9	**TS3-sn**	13.6
TS2-sx	13.9	**TS3-sx**	18.1
24	-25.0	**26**	-27.1
13	-31.1	**17**	-30.6
14	-30.3	**27**	-30.1
25	-25.2	**28**	-24.5

The thermodynamic data of the IIDA reaction of experimental dieniminium **12** were analysed. Relative enthalpies, entropies and Gibbs free energies, computed at 75 ºC in ethanol, are given in Table 5. Inclusion of the thermal corrections to the electronic energies in ethanol decreases the relative enthalpies between 0.1 and 4.0 kcal·mol^{-1}. The lower incidence is found in the relative enthalpies of the TSs which decreases by only 0.2 kcal·mol^{-1} with respect to the electronic energies. The inclusion of the thermal corrections and entropies to enthalpies increases the relative Gibbs free energies between 3.9 and 8.3 kcal·mol^{-1} as a consequence of the negative activation entropy associated to this intermolecular process, between −11.2 and −23.8 cal·mol^{-1}·K^{-1}. Thus, the activation Gibbs free energy associated to this IIDA reaction in ethanol rises to 12.6 kcal·mol^{-1}, while formation of **13** becomes exergonic by −20.5 kcal·mol^{-1}.

The activation enthalpy associated to the IIDA reaction via **TS2-rx** is 0.7 kcal·mol^{-1} higher than that associated to the intermolecular I-DA reaction via **TS1-n,** while the activation Gibbs free energy associated to the IIDA reaction is 12.7 kcal·mol^{-1} lower than that associated to the intermolecular I-DA reaction (see Table 3). The lower entropy loss taking place along the IIDA reaction of the experimental dieniminium **12**, −14.3 cal·mol^{-1}·K, than that associated to intermolecular process, −46.1 cal·mol^{-1}·K, is responsible for the high acceleration found in the intramolecular process.

Table 5. ωB97XD/6-311G(d,p) relative enthalpies (ΔH, in kcal·mol^{-1}), entropies (ΔS, in cal·mol^{-1}·K) and Gibbs free energies (ΔG, in kcal·mol^{-1}), with respect to the most stable conformation **12f**, computed at 75 ºC and 1 atm in ethanol, of the stationary points involved the IIDA reactions of dieniminium **12**.

	ΔH	ΔS	ΔG
12e	0.0	0.0	0.0
12f	-1.1	-11.2	2.8
TS2-rn	12.0	-16.2	17.6
TS2-rx	7.6	-14.3	12.6
TS2-sn	7.9	-16.6	13.7
TS2-sx	13.0	-14.5	18.1
24	-22.2	-23.8	-14.0
13	-28.5	-23.1	-20.5
14	-27.8	-20.9	-20.6
25	-22.3	-22.8	-14.4

The geometries of the TSs involved in the IIDA reaction of dieniminium **12f** are given in Figure 5, while those involved in the IIDA reaction of dieniminium **16f** are given in Figure S4 in Supplementary Material. The distances between the C2−C3 and N1−C6 interacting centers at the TSs involved in the IIDA reactions of dieniminium **12f** are found in a narrow range: between 1.93 and 1.98 Å (C2−C3) and 2.81 and 3.05 Å (N1−C6). Some appealing conclusions can be obtained for these geometrical parameters: i) these distances indicate that these TSs are associated to high asynchronous single bond formation processes; ii) the most favourable **TS2-rx** and **TS2-sn** are slightly more earlier; iii) these distances associated to the IIDA reaction are very closer to those found at the intermolecular I-DA reaction of butadiene **1** with ethaniminium **18** (see Figure 4); iv) while at the more favourable **TS2-rx** and **TS2-sn** the tetramethylene chain adopts a six-membered chair conformation, at the more unfavourable **TS2-rn** and **TS2-sx**, it adopt a boat-membered conformation. Consequently, the stereochemistry of these IIDA reactions is determined by the arrangement of the tetramethylene chain, thus justifying the total *re*/*exo* and *si*/*endo* facial diastereoselectivity found in these IIDA reactions with respect to low *endo* stereoselectivity found in I-DA reactions [13]; v) while the most favourable *re/exo* reaction path is associate to the formation of the *trans* quinolinium **13**, the *si/endo* reaction path is associate to the formation of the *cis* quinolinium **14**. These behaviours account for that formation of *trans* quinolinium **13** is 0.5 kcal·mol^{-1} more exergonic than formation of *cis* quinolinium **14**; and v) a comparison between the geometries of the TSs of the IIDA reactions of dieniminiums **12** and **16** indicates that the TSs associated with the reaction model are only slightly more advanced as less asynchronous than those associated to the experimental one (see Figure S4 in Supplementary Material).
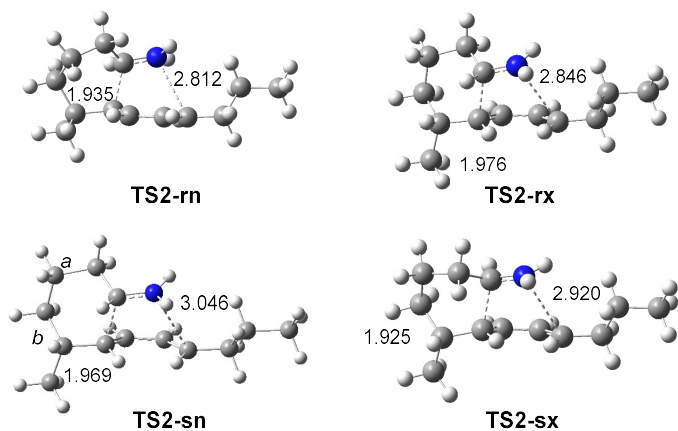

Figure 5. ωB97XD/6-311G(d,p) geometries of the TSs involved in the IIDA reaction of experimental dieniminium **12**. The C−C and C−N distances are given in Angstroms

The ionic nature of the IIDA reaction of dieniminium **12** was evaluated by computing the GEDT at the TSs. To this end, the natural atomic charges at the four TSs were shared in two groups through the two central Ca and Cb carbons of the tetramethylene chain (see Figure 5). The computed intramolecular GEDT values at the corresponding TSs, which fluxes from the nucleophilic butadiene framework to the superelectrophilic iminium one, are: 0.45 e (**TS2-rn**), 0.44 (**TS2-rx**), 0.43 (**TS2-sn**) and 0.49 (**TS2-sx**). These very high values, which are very similar to those obtained at the I-DA reaction of butadiene **1** with ethaniminium **18**, point out the high intramolecular GEDT taking place at these IIDA reactions.

3.3. Topological analysis of the bonding changes along the IIDA reactions

3.3.1. ELF analysis of the N1−C6 and C2−C3 single bond formation along the IIDA reaction of dieniminium 16

In order to characterize the formation of the two new N1−C6 and C2−C3 single bonds along the most favorable *re*/*exo* reaction path associated to the IIDA reaction of dieniminium **16**, and thus, to establish the molecular mechanism of these IIDA reactions, a topological analysis of the ELF of the three more relevant structures involved in the formation of the two new single bonds was performed. These three structures were selected from a Bonding Evolution Theory [52] (BET) study of the IIDA reaction of dieniminium **16**. The attractor positions of the ELF basins of the selected structures involved in this IIDA reaction are shown in Figure 6, while the complete BET study is gathered in Tables S7 in Supplementary Material.

The topology of the ELF of structure **S5**, d(N1-C6) = 2.840 and d(C2-C3) = 2.055 Å, shows the presence of a V(N1) monosynaptic basin, integrating 0.74 e, and two monosynaptic basins, V(C2) and V(C3), integrating 0.19 and 0.32 e, respectively. These monosynaptic basins, which are not present in dieniminium **16**, are created along reaction path. While the V(N1) monosynaptic basin, resulting of the strong depopulation of the N1−C2 bonding region and the intramolecular GEDT taking place in this IIDA reaction, is demanded for the formation of the N1−C6 single bond, the V(C2) and V(C3) monosynaptic basins are needed for the subsequent formation of the first C2−C3 single bond. At **S5**, the GEDT is 0.40 e.

At structure **S6**, d(N1-C6) = 2.822 and d(C2-C3) = 2.005 Å, while the two V(C2) and V(C3) monosynaptic basins present at structure **S5** have disappeared, a new V(C2,C3) disynaptic basin has been created with an initial population of 0.67 e (see Figure 6). These relevant topological changes indicate that the formation of the first C2−C3 single bond starts at a C−C distance of 2.01 Å by the merger of the non-bonding electron densities of the *pseudoradical* C2 and C3 centers present at structure **S5** [8]. The V(N1) monosynaptic basin present at **S5** has reached a population of 0.88 e. At **S6**, the GEDT is 0.45 e.

Finally, at structure **S7**, d(N1-C6) = 2.115 and d(C2-C3) = 1.580 Å, while the V(N1) monosynaptic basin present at structure **S6** has disappeared, a new V(N1,C6) disynaptic basin has been created with an initial population of 1.59 e (see Figure 6). These relevant topological changes indicate that the formation of the second N1−C6 single bond starts at a N−C distance of 2.11 Å, mainly by donation of the non-bonding electron density of the N1 nitrogen to the C6 carbon. Note that at the point of the IRC before to the structure **S6**, the V(N1) monosynaptic basin present at **S5** has reached a population of 1.59 e. At **S7**, the GEDT is 0.65 e.

At structure **S7**, the V(C2,C3) disynaptic basin created at **S6** has reached an electron density of 1.78 e, a value that represents the 93% of the electron density of the C2−C3 single bond at quinolinium **17**. This behaviour indicates that this IIDA reaction takes place through a non-concerted *two-stage one-step* mechanism [53].
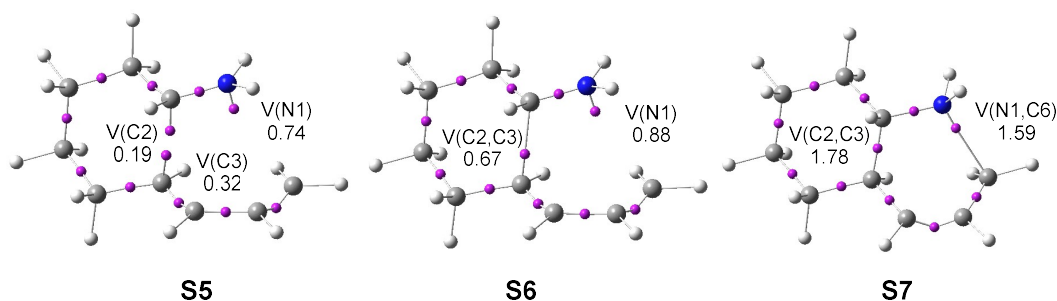

Figure 6. ELF basin attractor positions, with the most significant valence basin populations, in average number of e, of the structures involved in the formation of the N1−C6 and C2−C3 single bonds along the *re/exo* reaction path of the IIDA reaction of dieniminiums **16**

3.3.2. ELF and AIM comparative topological analysis of the most favorable TSs involved in the inter and intra I-DA reactions.

Finally, an ELF and AIM comparative topological analysis of the electronic structures of the most favorable *endo* TSs involved in the I-DA reaction of butadiene **1** with ethaniminium **18**, via **TS1-n**, and the IIDA reaction of dieniminium **16**, via **TS3-sn**, was performed in order to establish the similitude in both inter and intramolecular I-DA reactions. The attractor positions of the ELF basins of **TS1-n**, and **TS3-sn**, together with the population of the more relevant valence basins, and the presentations of the contour line maps of Laplacian $\nabla^2(r)$ of the electron density, together with the position of the critical points (CPs) associated to the C2−C3 and N1−C6 molecular regions, are shown in Figure 7, while the calculated AIM parameters of **CP1** and **CP2** are given in Table 6.

A comparison of the ELF of **TS1-n**, and **TS3-sn** shows that they have a great similitude. The iminium N1−C2 framework at both TSs is characterized by the presence of a V(N1,C2) disynaptic basin, integrating 2.70 and 2.60 e, respectively, and one V(N1) monosynaptic basin integrating 0.92 and 1.01 e. On the other hand, the butadiene moiety is characterized by the presence of three disynaptic basins, V(C3,C4), V(C4,C5) and V(C5,C7), integrating a total of 8.05 and 8.09 e. In addition, the two TSs show the presence of a V(C2,C3) disynaptic basin, integrating 0.84 and 0.88 e.

While the presence of the V(C2,C3) disynaptic basins at the two TSs indicates that the formation of the first C2−C3 single bond has begun yet at these TSs, the presence of the V(N1) monosynaptic basins, which have been created along the reaction paths, indicates that the formation of the second N1−C2 single bond has not begun.
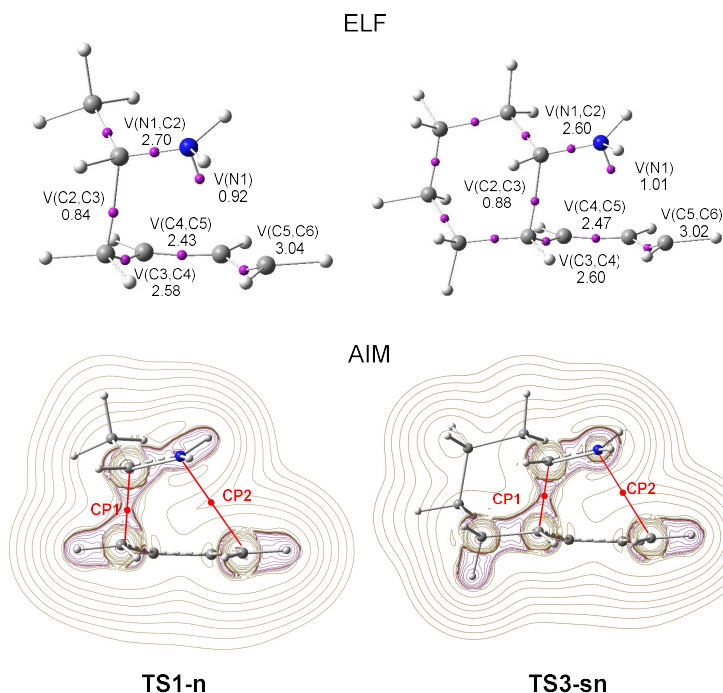
Figure 7. i) ELF basin attractor positions together with the most relevant valence basin populations at **TS1-n** and **TS3-sn**, and ii) Representations of the contour line maps of Laplacian $\nabla^2(r)$ of the electron density at **TS1-n** and **TS3-sn**. The **CP1** and **CP2** critical points are marked in the representations

Finally, the nature of the C2−C3 and N1−C6 electronic interactions at **TS1-n** and **TS3-sn** was studied by a AIM topological analysis of the electron density ρ at the (3,-1) CPs associated to the C2−C3 and N1−C6 molecular regions. The contour line maps of Laplacian $\nabla^2(r)$ of the electron density are shown in Figure 7, while the calculated AIM parameters are given in Table 6.

At **TS1-n**, **CP1** shows a negative Laplacian $\nabla^2(r)$ value, −0.0247, with an electron density of 0.0989, while **CP2** shows a positive Laplacian $\nabla^2(r)$ value, 0.0364, with a low electron density of 0.0142. Similarly, at **TS3-sn**, **CP1** shows a negative Laplacian $\nabla^2(r)$ value, −0.0274, with an electron density of 0.0989, while **CP2** shows a positive Laplacian $\nabla^2(r)$ value, 0.0444, with a low electron density of 0.0176. Thus, while at the two TSs, the negative Laplacian $\nabla^2(r)$ values of **CP1** indicate the presence of covalent interactions, the positive Laplacian $\nabla^2(r)$ values of **CP2** indicate the absence of covalent interactions

Espinosa [54] proposed a useful criterion to characterise interactions at the CPs, the ratio of potential kinetic energy electron density, |V(r)| / G(r). For ionic, non-covalent and

hydrogen bonding interactions, $|V(r)| / G(r) < 1$. Non-covalent interactions with somewhat covalent character is characterised by $1 < |V(r)| / G(r) < 2$, while covalent interactions show $|V(r)| / G(r) > 2$. The calculated values of $|V(r)| / G(r)$ at the selected CPs associated with **TS1-n** and **TS3-sn** are given in Table 6. The $|V(r)| / G(r)$ values of **CP1** at these TSs, between 2.18 and 2.21 au, indicate that they are associated to covalent interactions, while the $|V(r)| / G(r)$ values of **CP2**, between 0.85 and 0.88 au, indicate that they are associated to non-covalent interactions.

Table 6. AIM parameters, in au, of (3,-1) CPs at **TS1-n** and **TS3-sn** in the regions associated with the C−C and C−N single bond formation.

	TS1-n		TS3-sn	
	CP1	**CP2**	**CP1**	**CP2**
Density $\rho(r)$	0.0989	0.0142	0.1001	0.0176
Laplacian $\nabla^2(r)$	-0.0247	0.0364	-0.0274	0.0444
G(r)	0.0331	0.0079	0.0331	0.0099
V(r)	-0.0723	-0.0067	-0.0732	-0.0087
$|V(r)| / G(r)$	2.1843	0.8481	2.2115	0.8788
H(r)	0.0392	0.0012	0.0400	0.0012

The present ELF and AIM topological analysis of the electron density of **TS1-n** and **TS3-sn** shows that there is a complete similitude between the electronic structure of both TSs, in complete agreement with the similar geometries and GEDT of them.

Conclusions

The IIDA reactions of dieniminiums **12** and **16** have been studied within the MEDT at the DFT ωB97XD/6-311G(d,p) computational level. ELF topological analysis of dieniminiums **12** and **16** shows that the electronic structure of these species can be seen as the sum of those of butadiene **1** and that of ethaniminium **18**, joined by the tetramethylene chain. Analysis of the electrophilicity ω index of dieniminiums **12** and **16** points to the superelectrophilic character of these species. On the other hand, analysis of the Parr functions allows characterizing the most electrophilic centre, the iminium C2 carbon, and the most nucleophilic centres, the C3 and C6 carbons of the butadiene moiety, of dieniminium **16**.

The IIDA reaction of dieniminium **12** takes place via a one-step mechanism. The activation enthalpy associated to this IIDA reaction, 8.7 kcal·mol^{-1}, is closer to that of the I-DA reaction between butadiene **1** and ethaniminium **18**, 9.3 kcal·mol^{-1}. However, while the intermolecular I-DA reaction has an activation Gibbs free energy of 25.3 kcal·mol^{-1}, this IIDA reaction presents an activation Gibbs free energy of only 12.6 kcal·mol^{-1} as a consequence of the very low activation entropy associated to this intramolecular process, -14.3 cal·mol^{-1}·K. The strong exergonic character of the IIDA reaction, higher than 20.5 kcal·mol^{-1}, makes the reaction irreversible.

Unlike the I-DA reactions, which are low *endo* stereoselective [13], these IIDA reactions present a total *re/exo* and *si/endo* diastereoselectivity, which is controlled for the most favourable chair conformations adopted by the tetramethylene chain along the *re* and *si* intramolecular approaches. Such as in the I-DA reactions, the IIDA reaction of dieniminium **12** presents a very high intramolecular GEDT.

ELF topological analysis of the single bond formation along the IIDA reaction of dieniminium **16** indicates that it takes place through a non-concerted *two-stage one-step* mechanism. While formation of the first C2−C3 single bond begins by the merger of the non-bonding electron densities of the two *pseudoradical* C2 and C3 centers creates along the reaction path, formation of the second N1−C6 single bond begins mainly by the donation of the non-bonding electron density of the N1 nitrogen to the C6 carbon. Finally, ELF and AIM topological analyses of the more favorable TS associated to the I-DA reaction between butadiene **1** and ethaniminium **18**, and that associated to the IIDA reaction of dieniminium **16** show the great similitude of the two TSs.

The present MEDT study raises an interesting issue. The high GEDT taking place at the I-DA reactions is rationalised by the high $\Delta\mu$ values of the electronic chemical potentials μ of the two interacting species. Iminiums have very low electronic chemical potentials μ, lesser than -9.0 eV [13]. On the other hand, dieniminiums present electronic chemical potentials μ below -7.0 eV. The Sanderson's Electronegativity Equalisation Principle [55,56] establishes that along a polar interaction, the GEDT fluxes from the species with the high electronic chemical potentials μ to that with the low value. But, what happens in the intramolecular process for which MEDT recognize two distinguishable frameworks with electrophilic/nucleophilic properties similar to those present in intermolecular processes?

The answer to this question is that a regional descriptor for the electronic chemical potential μ_f for the different fragments of a molecule able to explain the GEDT taking place in intramolecular processes should be established.

References

1. Diels, O.; Alder, K. Synthesen in der hydroaromatischen Reihe. *Justus Liebigs Ann. Chem.* 1928, **460**, 98-122.

2. Carruthers, W. *Some Modern Methods of Organic Synthesis*. second ed., Cambridge University Press: Cambridge, 1978.

3. Carruthers, W. *Cycloaddition Reactions in Organic Synthesis*; Pergamon: Oxford, 1990.

4. Woodward, R. B.; Hoffmann, R. The Conservation of Orbital Symmetry *Angew. Chem. Int. Ed. Engl.* **1969**, *8*, 781-853.

5. Houk, K. N.; Gonzalez, J.; Li, Y. Pericyclic Reaction Transition States: Passions and Punctilios, 1935-1995. *Acc. Chem. Res.* **1995**, *28*, 81-90.

6. Rowley, D.; Steiner, H. Kinetics of diene reactions at high temperatures. *Discuss. Faraday Soc.* **1951**, *10*, 198-213.

7. Goldstein, E.; Beno, B.; K. N. Houk, K.N. Density Functional Theory Prediction of the Relative Energies and Isotope Effects for the Concerted and Stepwise Mechanisms of the Diels−Alder Reaction of Butadiene and Ethylene. *J. Am. Chem. Soc.* **1996**, *118*, 6036–6043.

8. Domingo, L.R. A new C-C bond formation model based on the quantum chemical topology of electron density. *RSC Adv.* **2014**, *4*, 32415–32428.

9. Domingo, L.R. Arnó, M., Andrés, J. Influence of Reactant Polarity on the Course of the Inverse-Electron-Demand Diels-Alder Reaction. A DFT Study of Regio- and Stereoselectivity, Presence of Lewis Acid Catalyst, and Inclusion of Solvent Effects in the Reaction between Nitroethene and Substituted Ethenes. *J. Org. Chem.* **1999**, *64*, 5867-5875.

10. Domingo, L.R.; Aurell, M.J.; Perez, P.; Contreras, R. Origin of the synchronicity on the transition structures of polar Diels-Alder reactions. Are these reactions [4+2] processes?. *J. Org. Chem.* **2003**, *68*, 3884-3890.

11. Domingo, L.R.; Sáez J.A. Understanding the mechanism of polar Diels–Alder reactions. *Org. Biomol. Chem.* **2009**, *7*, 3576-358.

12. Domingo, L.R. Molecular electron density theory: A modern view of reactivity in organic chemistry. *Molecules* **2016**, *21*, 1319.

13. Domingo, L.R.; Ríos-Gutiérrez, M.; Aurell, M.J. Unveiling the Ionic Diels-Alder Reactions within the Molecular Electron Density Theory. *Molecules* **2021**, 26, 3638.

14. Liang, Y.; Jiang, X.; Yu, Z.-X. Mechanisms of Cascade Reactions in the Syntheses of Camptothecin-Family Alkaloids: Intramolecular [4+ + 2]. Reactions of N-Arylimidates and Alkynes. *Org. Lett.* **2009**, *22*, 5303-5305.

15. Zhang, Y.; Zhu, Y.; Zheng, L.; Zhuo, l.-G.; Dang,Q.; Yu, Z.-X.; Bai, X. On-Demand Selection of the Reaction Path from Imino Diels–Alder to Ene-Type

Cyclization: Synthesis of Epiminopyrimido[4,5-b]azepines. *Eur. J. Org. Chem.* **2014**, 660–669.

16. Grieco P.A.; Parker, D.T. Octahydroquinoline Synthesis via Immonium Ion Based Diels-Alder Chemistry: Synthesis of (-)-8a-Epipumiliotoxin C. *J. Org. Chem.* **1988**, *53*, 3658-3662.

17. Chai, J.-D.; Head-Gordon, M. Long-range corrected hybrid density functionals with damped atom–atom dispersion corrections. *Phys. Chem. Chem. Phys.* **2008**, *10*, 6615-6620.

18. Hehre, M.J.; Radom, L.; Schleyer, P.v.R.; Pople, J. Ab initio Molecular Orbital Theory, Wiley, New York, 1986.

19. Schlegel, H.B. Optimization of equilibrium geometries and transition structures. *J. Comput. Chem.* **1982**, *3*, 214-218.

20. Schlegel, H.B. In modern electronic structure theory, Yarkony, D.R., Ed., World Scientific Publishing, Singapore, 1994.

21. Fukui, K. Formulation of the reaction coordinate. *J. Phys. Chem.* **1970**, *74*, 4161–4163.

22. González, C.; Schlegel, H. B. Reaction path following in mass-weighted internal coordinates. *J. Phys. Chem.* **1990**, *94*, 5523–5527.

23. González, C.; Schlegel, H. B. Improved algorithms for reaction path following: higher-order implicit algorithms. *J. Chem. Phys.* **1991**, *95*, 5853–5860.

24. Tomasi, J.; Persico, M. Molecular interactions in solution: and overview of methods based on continuous distributions of the solvent. *Chem. Rev.*, **1994**, *94*, 2027-2094.

25. Simkin, B.Ya.; Sheikhet, I.I. Quantum chemical and statistical theory of solutions–computational approach, Ellis Horwood: London, 1995.

26. Cossi, M.; Barone, V.; Cammi, R.; Tomasi, J. Ab initio study of solvated molecules: A new implementation of the polarizable continuum model. *Chem. Phys. Lett.*, **1996**, *255*, 327-335.

27. Cances, E.; Mennucci, B.; Tomasi, J. A new integral equation formalism for the polarizable continuum model: Theoretical background and applications to isotropic and anisotropic dielectrics. *J. Chem. Phys.*, **1997**, *107*, 3032-3041.

28. Barone, V.; Cossi, M.; Tomasi, J. Geometry optimization of molecular structures in solution by the polarizable continuum model. *J. Comput. Chem.* **1998**, *19*, 404-417.

29. Reed, A.E.; Weinstock, R.B.; Weinhold, F. Natural population analysis. *J. Chem. Phys.*, **1985**, *83*, 735-746.

30. Reed, A.E.; Curtiss, L.A.; Weinhold, F. Intermolecular interactions from a natural bond orbital, donor-acceptor viewpoint. *Chem. Rev.*, **1988**, *88*, 899-926.

31. Parr, R.G.; Yang, W. *Density functional theory of atoms and molecules*, Oxford University Press, New York, 1989.

32. Domingo, L.R.; Ríos-Gutiérrez, M.; Pérez, P. Applications of the conceptual density functional indices to organic chemistry reactivity. *Molecules* **2016**, *21*, 748.

33. Gaussian 16, Revision A.03, Frisch, M.J.; Trucks, G.W.; Schlegel, H.B.; Scuseria, G.E.; Robb, M.A.; Cheeseman, J.R.; Scalmani, G.; Barone, V.; Petersson, G. A.; Nakatsuji, H.; et al. Gaussian, Inc., Wallingford CT, **2016**.

34. Becke, A.D. Edgecombe, K.E. A simple measure of electron localization in atomic and molecular-systems. *J. Chem. Phys.* **1990**, *92*, 5397-5403.

35. Noury, S.; Krokidis, X.; Fuster, F.; Silvi, B. Computational tools for the electron localization function topological analysis. *Comput. Chem.* **1999**, *23*, 597-604.

36. Bader, R. F. W.; Tang, Y. H.; Tal, Y.; Biegler-König, F.W. Properties of atoms and bonds in hydrocarbon molecules *J. Am. Chem. Soc*. **1982**, *104*, 946-952.

37. Lu, T.; Chen, F. Multiwfn: A multifunctional wavefunction analyzer. *J. Comp. Chem*. **2012**, *33*, 580-592.

38. GaussView, Version 6.0, Dennington, R.; Keith, T.A.; Millam, J.M., Semichem Inc., Shawnee Mission, KS, **2016.**

39. Ahrens, J.; Geveci, B.; Law, C. ParaView: An End-User Tool for Large Data Visualization, Visualization Handbook, Elsevier, 2005, DOI:10.1016/B978-012387582-2/50038-1.

40. Ayachit, U. The ParaView Guide: A Parallel Visualization Application, Kitware, 2015, ISBN 978-1930934306.

41. Silvi, B.; Savin, A. Classification of chemical bonds based on topological analysis of electron localization functions. *Nature* **1994**, *371*, 683–686.

42. Pérez, P.; Domingo, L. R.; Aizman, A.; Contreras. R. The Electrophilicity Index in Organic Chemistry, In Theoretical Aspects of Chemical Reactivity. Toro-Labbe, A., Ed., Elsevier: Amsterdam, 2007, Vol. 9, pp 139−201.

43. Domingo, L.R.; Pérez, P. The Nucleophilicity N Index in Organic Chemistry. *Org. Biomol. Chem.* **2011**, *9*, 7168-7175.

44. Parr, R.G.; Pearson, R.G. Absolute hardness: Companion parameter to absolute electronegativity. *J. Am. Chem. Soc.* **1983**, *105*, 7512-7516.

45. Domingo, L.R. Mar Ríos-Gutiérrez, M.; Patricia Pérez, P.A Molecular Electron Density Theory Study of the Reactivity of Tetrazines in Aza-Diels-Alder Reactions. RSC Adv. 2020, 10, 15394–15405.

46. Parr, R.G. Szentpaly, L.v.; Liu, S. Electrophilicity index. *J. Am. Chem. Soc.* **1999**, *121*, 1922–1924.

47. Domingo, L.R.; Pérez, P., The Lithium Cation Catalysed Benzene Diels-Alder reaction. Insights on the Molecular Mechanism within the Molecular Electron Density Theory. *J. Org. Chem.* **2020**, *85*, 13121−13132.

48. Domingo, L.R.; Chamorro, E.; Pérez, P. Understanding the reactivity of captodative ethylenes in polar cycloaddition reactions. A theoretical study. *J. Org. Chem.* **2008**, *73*, 4615–4624.

49. Aurell, M. J.; Domingo, L.R.; Perez, P.; Contreras, R. A theoretical study on the regioselectivity of 1,3-dipolar cycloadditions using DFT-based reactivity indexes. *Tetrahedron*, **2004**, *60*, 11503-11509.

50. Domingo, L.R.; Perez, P.; Sáez, J. A. Understanding the local reactivity in polar organic reactions through electrophilic and nucleophilic Parr functions. *RSC Adv.* **2013**, *3*,1486-1494.

51. Domingo, L.R.; Rios-Gutierrez, M.; Ndassa, I.A.I.M.; Nouhou, C.N.; Mbadcam, J.K. Molecular Electron Density Theory Study of Fused Regioselectivity in the Intramolecular [3+2] Cycloaddition Reaction of Nitrones. *ChemistrySelect*, **2018**, *3*, 5412-5420.

52. Krokidis, X.; Noury, S.; Silvi, B. Characterization of Elementary Chemical Processes by Catastrophe Theory *J. Phys. Chem. A* **1997**, *101*, 7277–7282.

53. Domingo, L.R.; Sáez, J.A.; Zaragozá, R.J.; Arnó, M. Understanding the Participation of Quadricyclane as Nucleophile in Polar [$2\sigma + 2\sigma + 2\pi$] Cycloadditions toward Electrophilic π Molecules. *J. Org. Chem.,* **2008**, *73*, 8791-8799.

54. Espinosa, E.; Alkorta, I.; Elguero, J.; Molins, E. From weak to strong interactions: A comprehensive analysis of the topological and energetic properties of the electron density distribution involving X–H···F–YX–H···F–Y system *J. Chem. Phys*. **2002**, *117*, 5529-5542.

55. Sanderson, R. T. Partial charges on atoms in organic compounds. *Science* **1955**, *121*, 207-208.

56. Sanderson, R. T. Chemical Bonds and Bond Energy; 2nd ed.; Academic Press: New York, 1976.